Oncogene (2009) 28, 854–865

www.nature.com/onc

ORIGINAL ARTICLE

Merlin regulates transmembrane receptor accumulation and signaling at the plasma membrane in primary mouse Schwann cells and in human schwannomas

D Lallemand[1,2], J Manent[1,2], A Couvelard[3], A Watilliaux[1,2], M Siena[1,2], F Chareyre[1,2], A Lampin[1,2], M Niwa-Kawakita[1,2], M Kalamarides[1,2,4] and M Giovannini[1,2]

[1]INSERM, U674, Paris, France; [2]Université Paris 7, Denis Diderot, Institut Universitaire d'Hématologie, Paris, France; [3]APHP, Hôpital Beaujon, Service d'Anatomie et de Cytologie Pathologique, Clichy, France and [4]APHP, Hôpital Beaujon, Service de Neurochirurgie, Clichy, France

The *NF2* gene product, merlin/schwannomin, is a cytoskeleton organizer with unique growth-inhibiting activity in specific cell types. A narrow spectrum of tumors is associated with *NF2* deficiency, mainly schwannomas and meningiomas, suggesting cell-specific mechanisms of growth control. We have investigated merlin function in mouse Schwann cells (SCs). We found that merlin regulates contact inhibition of proliferation by limiting the delivery of several growth factor receptors at the plasma membrane of primary SCs. Notably, upon cell-to-cell contact, merlin downregulates the membrane levels of ErbB2 and ErbB3, thus inhibiting the activity of the downstream mitogenic signaling pathways protein kinase B and mitogen-activated protein kinase. Consequently, loss of merlin activity is associated with elevated levels of ErbB receptors in primary SCs. We also observed accumulation of growth factor receptors such as ErbB2 and 3, insulin-like growth factor 1 receptor and platelet-derived growth factor receptor in peripheral nerves of *Nf2*-mutant mice and in human NF2 schwannomas, suggesting that this mechanism could play an important role in tumorigenesis.
Oncogene (2009) **28,** 854–865; doi:10.1038/onc.2008.427; published online 24 November 2008

Keywords: neurofibromatosis type 2; growth factor receptors; trafficking; Schwann cells; proliferation; schwannoma

Introduction

Merlin is the product of the *NF2* tumor suppressor gene that shares strong sequence and structural homology with the ERM proteins (Ezrin, Radixin and Moesin), as well as the capacity to bind to F-actin and plasma membrane proteins (Bretscher *et al*., 2002). Merlin inhibits the proliferation of many different cell types, although the proposed mechanisms vary considerably. Merlin was shown to downregulate a wide range of mitogenic signaling pathways, such as Ras, Rac or PI3K (Fraenzer *et al*., 2003; Kissil *et al*., 2003; Lim *et al*., 2003; Hirokawa *et al*., 2004; McClatchey and Giovannini, 2005; Morrison *et al*., 2007). Moreover, *Nf2* inactivation results in destabilization of adherens junctions (AJs) that are essential for contact inhibition of proliferation in mouse embryonic fibroblasts (MEFs) (Lallemand *et al*., 2003). In addition, merlin can block ligand-induced epidermal growth factor receptor internalization and signaling in various cell types (Curto *et al*., 2007). In a rat schwannoma cells, merlin also inhibits growth by promoting platelet-derived growth factor receptor (PDGFR) degradation (Fraenzer *et al*., 2003). Finally, in *Drosophila*, D-Merlin and Expanded cooperate to stimulate endocytosis of membrane proteins, such as Notch and epidermal growth factor receptor, thereby reducing their levels at the cell surface and inhibiting downstream signaling (Maitra *et al*., 2006). Despite these pieces of evidence, there is no consensus as to whether these mechanisms are central to specific NF2-related tumors. One striking feature of NF2 is the narrow tumor spectrum composed essentially of benign schwannomas and meningiomas. Therefore, we decided to study merlin function in mouse Schwann cells (SCs) that are most likely to provide pertinent information about the molecular mechanisms of NF2 tumor suppression.

Large cultures of primary SC can be derived from mice harboring a conditional *Nf2* allele (Giovannini *et al*., 2000; Manent *et al*., 2003). In these cells, *Nf2* is inactivated following adenovirus-mediated Cre expression, allowing the study of the early consequences of merlin loss on SC proliferation and tumor initiation. We found that merlin controls contact-dependent inhibition of SC proliferation by inhibiting the delivery of receptors to the plasma membrane. Notably, merlin downregulates the membrane levels of ErbB2 and ErbB3, thus inhibiting downstream mitogenic signaling pathways. Moreover, we show that loss of merlin

Correspondence: Dr M Giovannini, House Ear Institute, Center for Neural Tumor Research, 2100W Third Street, Los Angeles, CA 90057, USA.
E-mail: mgiovannini@hei.org
Received 19 March 2008; revised 10 September 2008; accepted 15 September 2008; published online 24 November 2008

activity is associated with elevated levels of ErbB receptors in peripheral nerves of *Nf2*-mutant mice as well as in human NF2 schwannomas. Taken together, our data suggest that the altered delivery of ErbB receptors plays a major role in schwannoma development.

Results

Proliferative advantage of Nf2$^{-/-}$ *SCs*

We did not observe any difference in the growth rates between *Nf2*$^{+/+}$ and *Nf2*$^{-/-}$ SCs as long as they remained subconfluent (Supplementary Figure 1). Once *Nf2*$^{+/+}$ SC cultures reached confluence, we saw progressive growth arrest between days 5 and 13 of culture (Figure 1a). In contrast, *Nf2*$^{-/-}$ SCs kept growing and reached saturation densities 2–3 times higher than *Nf2*$^{+/+}$ SCs (Figures 1a–c). Adenovirus-mediated re-expression of merlin was sufficient to restore saturation densities similar to those observed in *Nf2*$^{+/+}$ SCs, illustrating that loss of merlin was responsible for the phenotype (Figures 1b and c).

Primary cells in culture undergo progressive and irreversible growth arrest after several passages, a process referred to as replicative senescence. Primary mouse cells can escape this fate by losing expression of tumor suppressor genes, such as *p21*^{Cip}, *p53* or *pRb* (Bringold and Serrano, 2000; Itahana *et al*., 2004). We observed that *Nf2*$^{+/+}$ SCs became senescent after five to seven passages in culture when they stopped proliferating, lost their bipolar shape and became very large and flat, the typical morphological features of senescent cells (Figures 1d and e). In contrast, *Nf2*$^{-/-}$ SCs never stopped proliferating (Figure 1d) and showed none of the morphological features of senescence (Figure 1e). Although levels of p107, p130, p53, p19^{Arf} and p21^{Cip} increased in late-passage *Nf2*$^{-/-}$ SCs, their expression levels remained always lower than in *Nf2*$^{+/+}$ SC (Figure 1f). p27^{Kip} levels were not affected by *Nf2* inactivation. Beyond passage 8, *Nf2*$^{-/-}$ SCs never became senescent and spontaneously transformed.

Transmembrane receptors accumulate at the plasma membrane of Nf2*-deficient SCs*

Following *Nf2* inactivation in SCs, we observed a clear morphological change (Figure 2a, upper panels) and profound alterations of the actin cytoskeleton (Figure 2a, lower panels), suggesting that, as in MEFs (Lallemand *et al*., 2003), *Nf2* inactivation results in the loss of cell–cell contact. AJs were visualized by staining of β-catenin, a component of these structures. In contrast to *Nf2*$^{+/+}$ SCs, staining of β-catenin in *Nf2*-deficient SCs was not clearly localized in regions of cell–cell contact (Figure 2a, middle panels). These observations suggest that upon merlin loss, junctional components are expressed but not properly localized. Next, we investigated whether loss of merlin expression modified the abundance or localization of other plasma membrane proteins involved in SC proliferation, such as growth factor and adhesion receptors. We found that the amounts of several growth factor receptors (ErbB2, ErbB3, insulin-like growth factor 1 receptor (IGF1R), PDGFR-β) and adhesion molecules (N- and E-cadherin) were elevated in total membrane extracts from confluent *Nf2*$^{-/-}$ SCs compared with *Nf2*$^{+/+}$ SCs, whereas β-catenin levels were not (Figure 2b). These observations were confirmed by surface protein biotinylation (Figure 2d). In contrast, receptor levels were nearly identical in subconfluent *Nf2*$^{+/+}$ SCs and *Nf2*$^{-/-}$ SCs (Supplementary Figure 2). Quantification of the signals showed that the higher levels of receptors were associated with an increase of phosphorylated receptors. These molecular phenotypes were strictly regulated by merlin because its reintroduction into *Nf2*$^{-/-}$ SCs markedly reduced the levels of ErbB2, ErbB3, IGF1R, PDGFR-β and E- and N-cadherin at the plasma membrane (Figures 2c and d). Quantification of specific markers EEA1, Lamp1, p115 or Rab11 in membrane extracts by western blot (Figure 2e) and by immunofluorescence staining (Supplementary Figure 3) suggested that the accumulation of membrane proteins in *Nf2*$^{-/-}$ SCs was not the result of an expansion of intracellular compartments, such as the Golgi apparatus or the endocytic vesicles. In addition, saturation of the plasma membrane with the lipophilic fluorescent dye FM1-43X demonstrated that this compartment was not enlarged in *Nf2*$^{-/-}$ SCs (Figure 2f). Finally, quantitative reverse transcription–PCR (RT–PCR) analysis showed no increase of *ErbB2*, *ErbB3* and *IGF1R* mRNA expression levels in *Nf2*$^{-/-}$ SCs and a slight increase of *Pdgfrb* (1.3-fold). Only *N-cadherin* mRNA levels were increased following loss of merlin expression (Figure 2g). In conclusion, *Nf2* inactivation in SCs leads to the accumulation of growth factor receptors at the plasma membrane, which is not due to increased protein synthesis.

Merlin regulates the delivery of growth factor receptors to the plasma membrane in SCs

Several reports have proposed a role for merlin in protein transport (Maitra *et al*., 2006; Curto *et al*., 2007) and the involvement of the ERM proteins in vesicular trafficking is well established (Pujuguet *et al*., 2003; Tamma *et al*., 2005; Stanasila *et al*., 2006). We compared growth factor internalization in *Nf2*$^{+/+}$ and *Nf2*$^{-/-}$ SC cultures using a surface protein biotin pulse-chase approach and found no differences (data not shown). As the phenotype might be too subtle to be detected using this method, we decided to overexpress merlin in *Nf2*$^{-/-}$ SCs to accentuate a putative trafficking defect. We observed no difference in the rate of internalization of the receptors 20 min after the biotin pulse (or at later times) when comparing *Nf2*$^{-/-}$ SCs with *Nf2*$^{-/-}$ SCs overexpressing merlin (*Nf2*$^{-/-;adNF2}$) (Figure 3a). Secondly, we investigated the rate of degradation of surface receptors in *Nf2*$^{-/-}$ and *Nf2*$^{-/-;adNF2}$ SCs, and again found no difference (Figure 3b). Next, we explored the role of merlin in vesicular transport from the Golgi apparatus to the

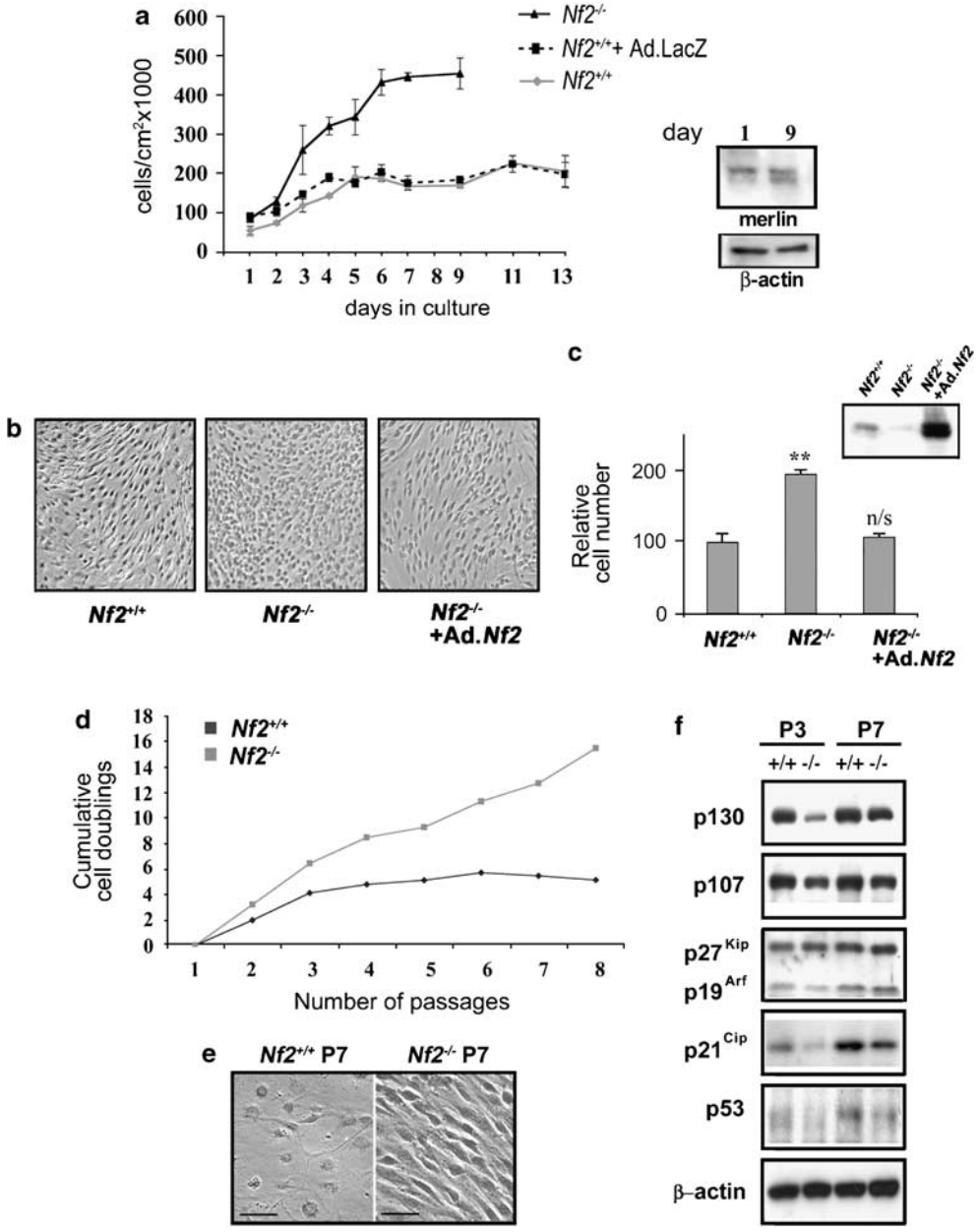

Figure 1 Proliferation of *Nf2*-deficient Schwann cells (SCs). (**a**) Growth curve of confluent $Nf2^{+/+}$ and $Nf2^{-/-}$ primary SCs. Cells were seeded at 7.5×10^4/cm² and counted daily. LacZ-expressing adenovirus was used as a control for adverse effects of adenoviral infection. The density reached by $Nf2^{-/-}$ SCs was so high that cells could not be trypsinized to single-cell levels beyond day 9 and counting became too imprecise. The western blots show the increase of hypophosphorylated active merlin (lower band) when $Nf2^{+/+}$ SCs reach high density (day 9). (**b**) Phase contrast pictures of saturated cultures of $Nf2^{+/+}$ (left), $Nf2^{-/-}$ (middle) and $Nf2^{-/-}$ SCs re-expressing merlin isoform I (right). $Nf2^{-/-}$ SCs were infected 24 h after plating, with merlin- or LacZ-expressing adenovirus for control ($Nf2^{-/-}$). Pictures were taken 10 days after infection. (**c**) Cell saturation densities corresponding to images of panel (**b**). The western blot shows merlin expression in $Nf2^{+/+}$, $Nf2^{-/-}$ and $Nf2^{-/-}$ SCs re-expressing merlin isoform I ($Nf2^{-/-}$ + Ad.*Nf2*). (**d**) Cumulative numbers of doublings of $Nf2^{+/+}$ and $Nf2^{-/-}$ primary SCs. (**e**) Phase contrast picture of $Nf2^{+/+}$ and $Nf2^{-/-}$ primary SCs at passage 7. Scale bars = 10 μm. (**f**) Western blot analysis of the expression of senescence markers (P107, P130, $P27^{Kip}$, $P21^{Cip}$, $P19^{Arf}$ and p53) from extracts of primary $Nf2^{+/+}$ and $Nf2^{-/-}$ SCs at early (P3) and late (P7) passage.

plasma membrane (Figure 3c). We took advantage of the temperature-sensitive mutant of the viral VSVprotein (ts045VSV) fused to the green fluorescent protein (GFP) that has been widely used for these types of studies (Hirschberg *et al*., 1998; Siskova *et al*., 2006). At 40 °C, the ts045VSV-GFP protein is misfolded and retained in the endoplasmic reticulum. At 32 °C, the fusion protein folds properly, synchronously moves to the Golgi apparatus and is transported to the plasma membrane where its accumulation can be followed using surface protein biotinylation. In myoblasts, N-cadherin and ts045VSV-GFP colocalized in secretory vesicles (Mary *et al*., 2002). Similarly, ErbB2, ErbB3, IGF1Rβ and PDGFR-β colocalized with ts045VSV-GFP in

secretory vesicles in SCs (Figure3d and supplementary Figure 4). Therefore, ts045VSV-GFP most likely represents an accurate model for the transport of cadherins and growth factor receptors to the cell surface. Figure 3c demonstrated that ts045VSV-GFP protein accumulation at the plasma membrane was inhibited by merlin overexpression. The presence of a cleavage product of ts045VSV-GFP in total extracts from $Nf2^{-/-;adNF2}$ (arrow in Figure 3c, right panel) suggested that some of the protein that is not delivered to the plasma membrane was targeted for degradation. In conclusion, merlin controls the amount of adhesion and growth factor receptors at the cell surface of SCs by inhibiting their delivery to the plasma membrane.

Accumulation of the ErbB receptors at the plasma membrane confers a growth advantage to SCs

Our observations suggested that increased levels of growth factor receptors at the plasma membrane of $Nf2^{-/-}$ SCs stimulate downstream mitogenic pathways and trigger proliferative advantage. Heregulin-β1, the ligand for ERbB3, is the only growth factor present in the define media that we used for primary SC cultures. When heregulin-β1 concentration was lowered, ErbB receptor activity decreased and contact inhibition was restored in $Nf2^{-/-}$ SC (Figure 4a). A sharp decrease of the replication potential (Figure 4b) and the induction of a senescent morphology similar to that of $Nf2^{+/+}$ SC at the same passage (compare phase contrast images in Figure 4b and Figure 1e) were also observed. In contrast, reducing the concentration of insulin had no effect on the proliferation rate (data not shown) or the replicative potential of $Nf2^{-/-}$ SC (Figure 4b). These data strongly suggested that the increased saturation density of $Nf2^{-/-}$ SCs was the consequence of the accumulation of ErbB receptors. Western blot analysis showed that mitogen-activated protein kinase (MAPK) and protein kinase B (Akt) pathways were activated in confluent $Nf2^{-/-}$ SC (Figure 4c). Reducing heregulin-β1 concentration in $Nf2^{-/-}$ SC cultures resulted in lower levels of phosphorylated Akt and MAPK. Conversely, overexpressing human ErbB2 (HER2) in $Nf2^{+/+}$ SCs stimulated MAPK and Akt phosphorylation and activity (Figure 4d). Finally, specific inhibition of ErbB2, MEK/MAPK or PI3K/Akt leads to a drastic reduction of $Nf2^{-/-}$ SC proliferation (Figure 4e), showing that these pathways are essential for SC proliferation in culture. In conclusion, we found that the cell surface accumulation of ErbB receptors at confluence in $Nf2^{-/-}$ SCs stimulates mitogenic MAPK and PI3K/Akt pathways leading to persistent proliferation and increased saturation densities.

Increased levels of growth factor receptors in Nf2*-mutant mouse peripheral nerves and in human schwannomas*

To test whether the accumulation of receptors that we observed in $Nf2^{-/-}$ SCs was relevant for tumor formation, we analysed the expression of growth factor receptors in mouse peripheral nerves. We found that ErbB3, IGF1R and PDGFR-β expression levels were elevated in *Nf2*-mutant peripheral nerves as compared with wild-type nerves (Figures 5a and b). N-cadherin levels were also increased (Figure 5a). Strikingly, the overall pattern of membrane protein accumulation in *Nf2*-mutant peripheral nerves, before the development of tumors, matched the pattern we described in $Nf2^{-/-}$ SCs. This observation showed that the molecular consequences of loss of merlin expression in SCs are context independent. Next, we compared the expression levels of several plasma membrane proteins in a series of eight human schwannomas that did not express merlin (five from sporadic tumors and three from NF2 patients) and in three normal human nerves. Western blot analysis (Figure 5c) showed that, as for mouse *Nf2*-mutant nerves, levels of HER2, HER3, IGF1R, PDGFR-β and N-cadherins were clearly elevated in schwannomas. Accordingly, immunohistochemical analysis of HER2, HER3, PDGFR-β and N-cadherins showed strong immunostaining on tumor tissue and a weaker staining pattern in control nerves (Figure 5d). Differences in HER2, HER3 and N-cadherin expression in a series of 30 human schwannomas and 8 normal nerves were quantified by scoring staining intensities. Statistically significant differences between normal nerves and schwannomas were observed for HER2, HER3 and N-cadherin (Figure 5e). mRNA expression levels of *HER2, HER3, IGF1R* and *PDGFR-β* genes were not significantly increased in human schwannomas compared with normal nerves (Figure 5f). In contrast, *N-cadherin* mRNA expression was upregulated in human schwannomas as it was in mouse $Nf2^{-/-}$ SC cultures. These observations strengthen our hypothesis that deregulated transport is responsible for the accumulation of growth factor receptors in human schwannomas.

In conclusion, loss of merlin expression results in the accumulation of growth factor receptors at the plasma membrane of SCs. As it is a major mechanism of the proliferative advantage of $Nf2^{-/-}$ SCs *in vitro*, it may represent an important step in the initiation of schwannoma development in mouse NF2 models and in NF2 patients.

Discussion

Although regulation of merlin activity is well understood, the mechanisms of its tumor suppressive function remain elusive (McClatchey and Giovannini, 2005). AJs are central to the process of contact inhibition of cell growth. Upon cadherin engagement, the activity of receptors tyrosine kinases and downstream mitogenic signaling pathways is progressively inhibited (Qian *et al*., 2004; Perrais *et al*., 2007). The mislocalization of some of the AJ components in confluent $Nf2^{-/-}$ SCs indicates that AJs might be dysfunctional in SCs. Nevertheless, the fact that lowering the concentration of heregulin-β1 restored contact inhibition in $Nf2^{-/-}$ SCs suggested that AJs could still contribute to growth inhibition in these cells. Our data support the hypothesis

that in $Nf2^{-/-}$ SCs, AJs cannot efficiently inhibit the elevated mitogenic signaling arising from increased ErbB levels and that the net result of the antagonistic relationship between receptors tyrosine kinases and AJs is shifted toward promitogenic signaling. We found that, in SCs, merlin regulates the expression of various receptors at the cell surface. These observations agree with the function proposed for merlin in *Drosophila*

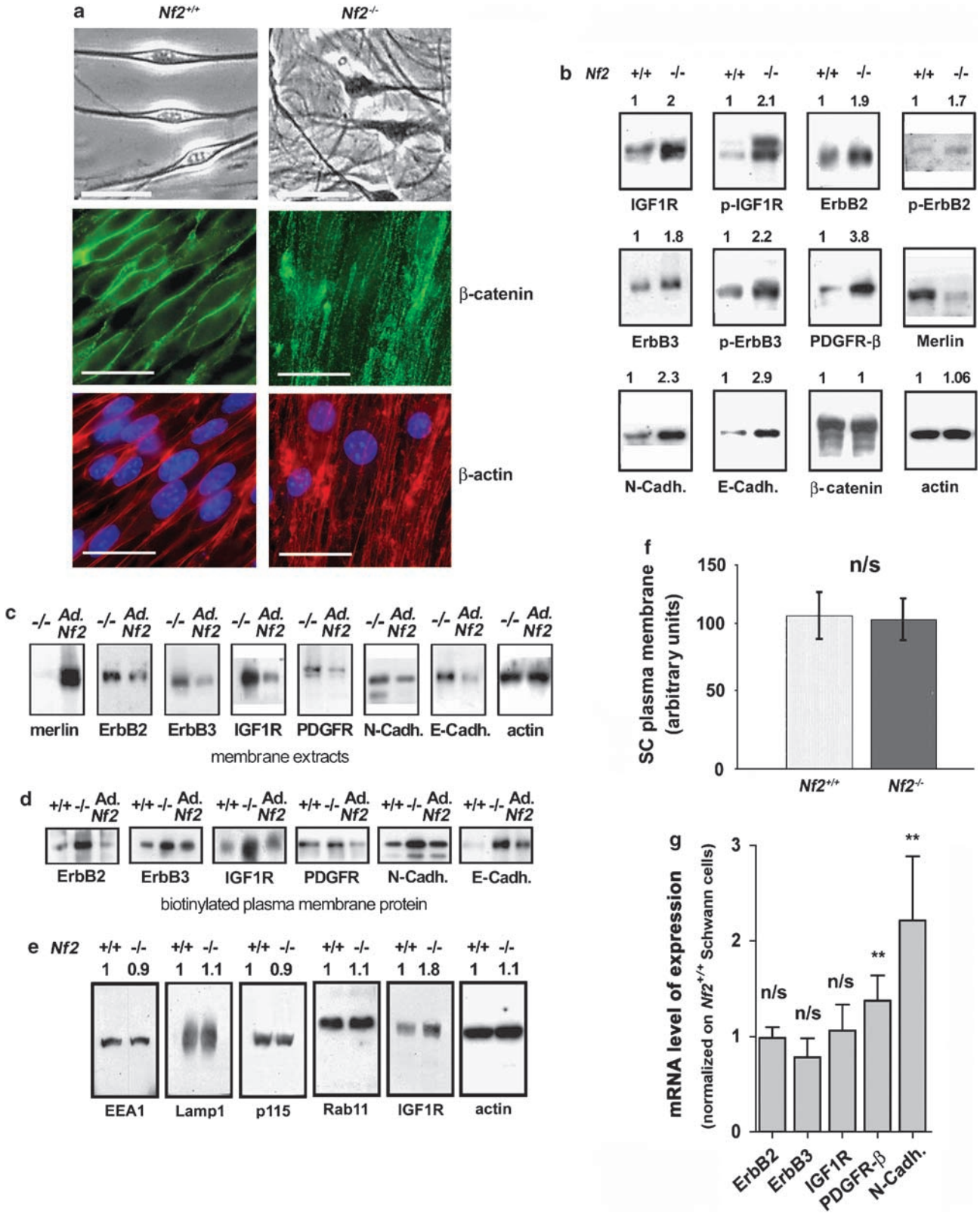

where the combined loss of *D-Merlin* and the tumor suppressor *Expanded* in the eye results in the accumulation of several membrane proteins (Maitra *et al*., 2006). Although merlin and Expanded modulate growth factor receptor internalization in *Drosophila*, our data indicate that, in SCs, merlin inhibits the delivery of proteins to the plasma membrane. This difference could be accounted for by the concomitant *Expanded* inactivation in *Drosophila*, as single *D-Merlin* or *Expanded* inactivation did not affect internalization. Tissue-specific factors could also explain the differences across species, as in MEFs, osteoblasts and liver-derived cells, merlin inhibits epidermal growth factor receptor internalization upon cell–cell contact preventing the activation of downstream signaling pathways (Curto *et al*., 2007).

Following release from the Golgi apparatus, the ts045VSV-GFP construct is partially degraded in merlin-expressing SC, suggesting that a fraction of the protein pool was directly targeted for degradation. Interestingly, in a schwannoma cell line, merlin regulates membrane levels of PDGFR-β by inducing its degradation (Fraenzer *et al*., 2003), revealing an additional degree of complexity in merlin regulation of growth factor steady state levels. ERM proteins also are implicated in vesicular trafficking (Pujuguet *et al*., 2003; Deretic *et al*., 2004; Stanasila *et al*., 2006). Thus, merlin and ERM proteins regulate protein transport to and from the plasma membrane. The fact that ERM proteins do not compensate for merlin loss suggests that they control independent pathways. How merlin modulates the delivery of proteins to the plasma membrane remains unknown. Interestingly, membrane fusion of secretory vesicles requires localized actin remodeling. In some cases actin acts as a physical barrier preventing the access to the plasma membrane (Muallem *et al*., 1995; Miyake *et al*., 2001). The severe actin disorganization induced by merlin loss (Figure 2a) might facilitate vesicle fusion with the plasma membrane and protein delivery. Alternatively, merlin could spatially restrict growth factor receptors and adhesion molecules accumulation within the plasma membrane. In SCs, it has been reported that merlin interacts with ErbB2 hence controlling its subcellular localization (Fernandez-Valle *et al*., 2002). Therefore, loss of merlin expression could allow for a broader distribution of membrane-associated proteins. From our study and others, it appears that merlin regulates growth factor receptor presence at the plasma membrane of confluent cells in several ways. The different mechanisms proposed may reflect the predominance of a particular merlin function in a specific organism or cell type, and underscore the relevance of using SC in our study for the understanding of human schwannomagenesis. We have also presented strong evidence that ErbB-mediated activation of downstream mitogenic signaling pathways is important for schwannoma development. *In vitro*, expression of a constitutively activated form of ErbB2 in rat SC promotes transformation (Sherman *et al*., 1999). *In vivo*, chemically induced activating mutations of ErbB2 trigger malignant schwannoma development in rodents (Nikitin *et al*., 1991; Buzard *et al*., 1999). Thus, it appears that in SC, strong activation of ErbB signaling due to an oncogenic mutation of ErbB2 promotes malignant tumorigenesis, whereas a milder activation following the accumulation of wild-type ErbB receptors results in a benign tumorigenic process. Surprisingly, no oncogenic ErbB2 mutations have been ever found in human schwannomas.

Our study shows that expression levels of growth factor receptors known to be involved in SC proliferation and survival are increased in peripheral nerves isolated from two different types of *Nf2*-mutant mice. Moreover, protein expression analysis performed on schwannoma biopsies convincingly showed increased levels of the corresponding ortholog proteins, notably HER2 and HER3. These results support the hypothesis that schwannoma development in NF2 patients is linked to the accumulation of ErbBs receptors. This conclusion is reinforced by several studies that show upregulation and activation of ErbBs and downstream signaling pathways, such as PI3K/Akt and MAPK, in schwannomas (Hansen and Linthicum, 2004; Stonecypher *et al*., 2006). Although ErbB signaling is most likely to play a key role in schwannoma development, IGF1R and PDGFR-β are also involved in SC survival and

Figure 2 Growth factor and adhesion receptors accumulate at the plasma membrane of *Nf2*-deficient Schwann cells (SCs). (**a**) Upper two panels: phase contrast micrographs of $Nf2^{+/+}$ and $Nf2^{-/-}$ subconfluent primary SCs. Scale bars = 10 μm. Middle two panels: β-catenin staining of fixed confluent primary $Nf2^{+/+}$ and $Nf2^{-/-}$ SCs (green) and 4,6-diamidino-2-phenylindole (DAPI) (blue). Scale bars = 5 μm. Lower two panels: rhodamine-phalloidin staining of actin in the same field (red) and DAPI (blue). Scale bars = 5 μm. (**b**) Western blot analysis of total and phosphorylated growth factor receptors levels (insulin-like growth factor 1 receptor (IGF1R), ErbB2 and 3 and platelet-derived growth factor receptor (PDGFR)-β) and adhesion molecules (N-cadherin, E-cadherin and β-catenin) in membrane extracts from early confluent $Nf2^{+/+}$ and $Nf2^{-/-}$ primary SCs at passage 3. Actin was used as a loading control and lack of merlin expression in $Nf2^{-/-}$ SC was confirmed. Quantification of the signals is presented and was normalized to the wild-type SC signal after correction from the actin control. (**c**) Re-expression of merlin in $Nf2^{-/-}$ SC resulted in downregulation of ErbB2, ErbB3, IGF1R, PDGFR-β, E- and N-cadherin levels. (**d**) Elevated plasma membrane levels of E- and N-cadherin, ErbB2, ErbB3, PDGFR-β and IGF1R in confluent $Nf2^{-/-}$ SCs (−/−) compared with $Nf2^{+/+}$ SC (+/+) was confirmed by surface protein biotinylation. Overexpression of merlin (Ad.*Nf2*) in $Nf2^{-/-}$ SCs restored membrane levels of these proteins similar to $Nf2^{+/+}$ SC. (**e**) Expression of subcellular compartment markers in total membrane extracts from $Nf2^{+/+}$ and $Nf2^{-/-}$ SCs: early endosome (EEA1), lysosome (Lamp1), Golgi (p115), late endosome (Rab11). Levels of IGF1R are shown for comparison. Quantification of the signals has been normalized to the wild-type SC signal and corrected from the actin control. (**f**) Quantification of the plasma membrane compartment: plasma membrane of $Nf2^{+/+}$ and $Nf2^{-/-}$ SCs were saturated with the fluorescent lipophilic dye FM1-43FX and fluorescence was quantified by flow-cytometry. (**g**) *ErbB2, ErbB3, IGF1R, PDGFR-β* and *N-cadherin* mRNA expression in $Nf2^{-/-}$ primary SCs relative to $Nf2^{+/+}$(data represent mean ± s.e.m.).

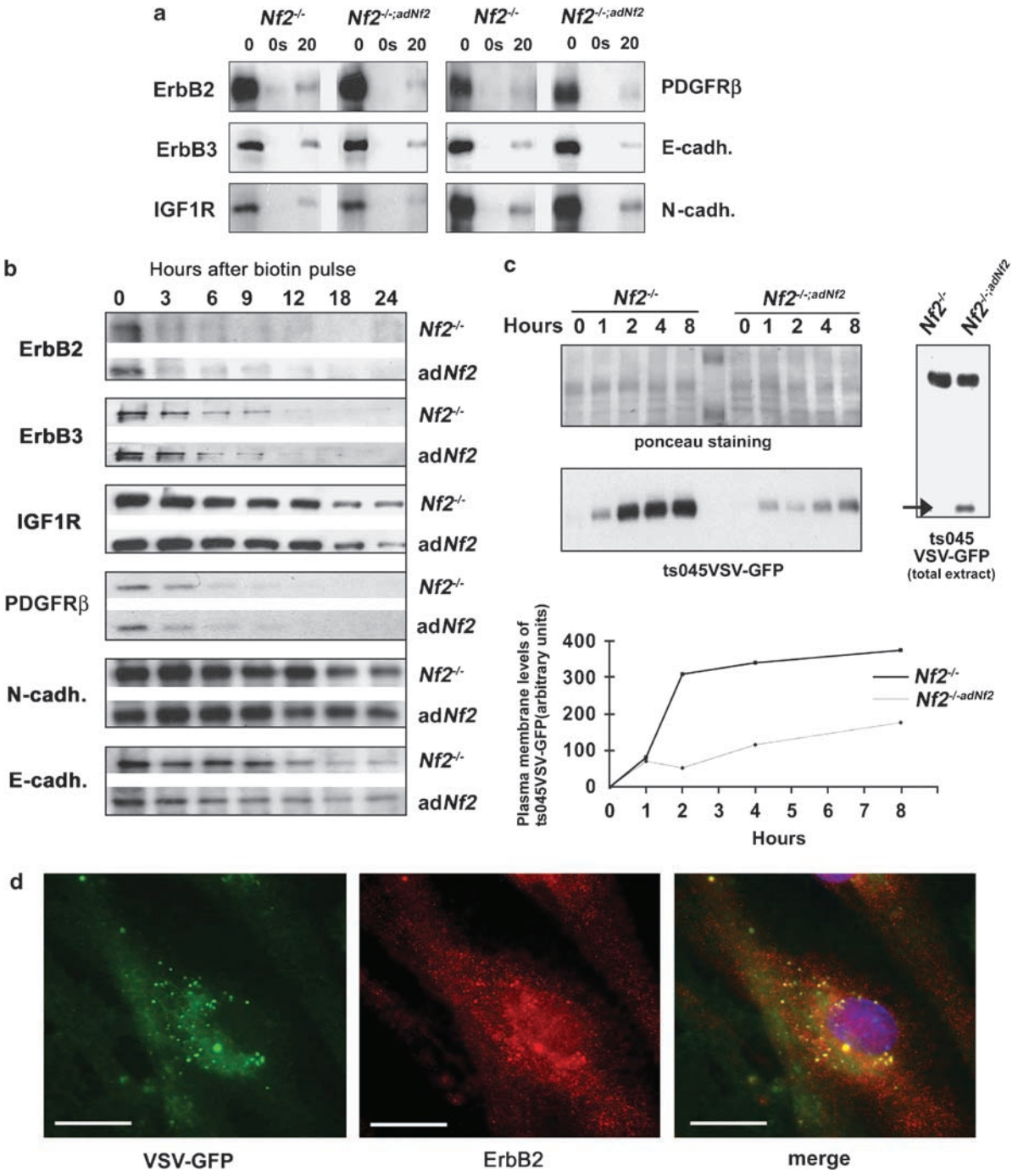

Figure 3 Merlin inhibits delivery of proteins to the plasma membrane. (**a**) Kinetics of ErbB2, ErbB3, insulin-like growth factor 1 receptor (IGF1R), platelet-derived growth factor receptor (PDGFR)-β and E- and N-cadherin internalization in $Nf2^{-/-}$- and $Nf2^{-/-}$-overexpressing merlin isoform I ($Nf2^{-/-;adNf2}$) primary Schwann cells (SCs). The first lane (0) represents the receptors exposed at the cell surface immediately following biotin pulse (T = 0 min). The second lane (0s) represents the receptors that have been internalized at $T = 0$ min. The third lane (20) represents the receptors that have been internalized 20 min after the biotin pulse. (**b**) Western blot analysis showing the progressive clearance of biotinylated ErbB2, ErbB3, IGF1R, PDGFR-β and E- and N-cadherin from $Nf2^{+/+}$ and $Nf2^{-/-;adNf2}$ SCs over 24 h. (**c**) (Upper left): western blot analysis of the accumulation of the ts045VSV-green fluorescent protein (GFP) at the plasma membrane of $Nf2^{-/-}$ and $Nf2^{-/-;adNf2}$ SCs (lower panel). Equal loadings of biotinylated proteins were assessed by ponceau staining (upper panel). Upper right: ts045VSV-GFP expression in total cell extracts show a 20% decrease in $Nf2^{-/-;adNf2}$ SCs and the presence of a cleavage product (arrow). Bottom: graphic representation of the kinetic of ts045VSV-GFP transport to the plasma membrane. Western blot was scanned and quantified using imageQ software. The relative abundance of ts045VSV-GFP has been corrected from the lower total amount of ts045VSV-GFP present in $Nf2^{-/-;adNf2}$ SC extracts. (**d**) ts045VSV-GFP and ErbB2 colocalize in vesicles following their release from the Golgi (scale bars = 2 μm). Primary SCs expressing ts045VSV-GFP were treated overnight with 3 μg/ml of brefeldin A, a drug that blocks the release of newly synthesized proteins from the Golgi. Following the release from the block, progression of ts045VSV-GFP and ErbB2 in transport vesicles was followed by immunofluorescence. Colocalization with several other receptors is presented in Supplementary Figure 4.

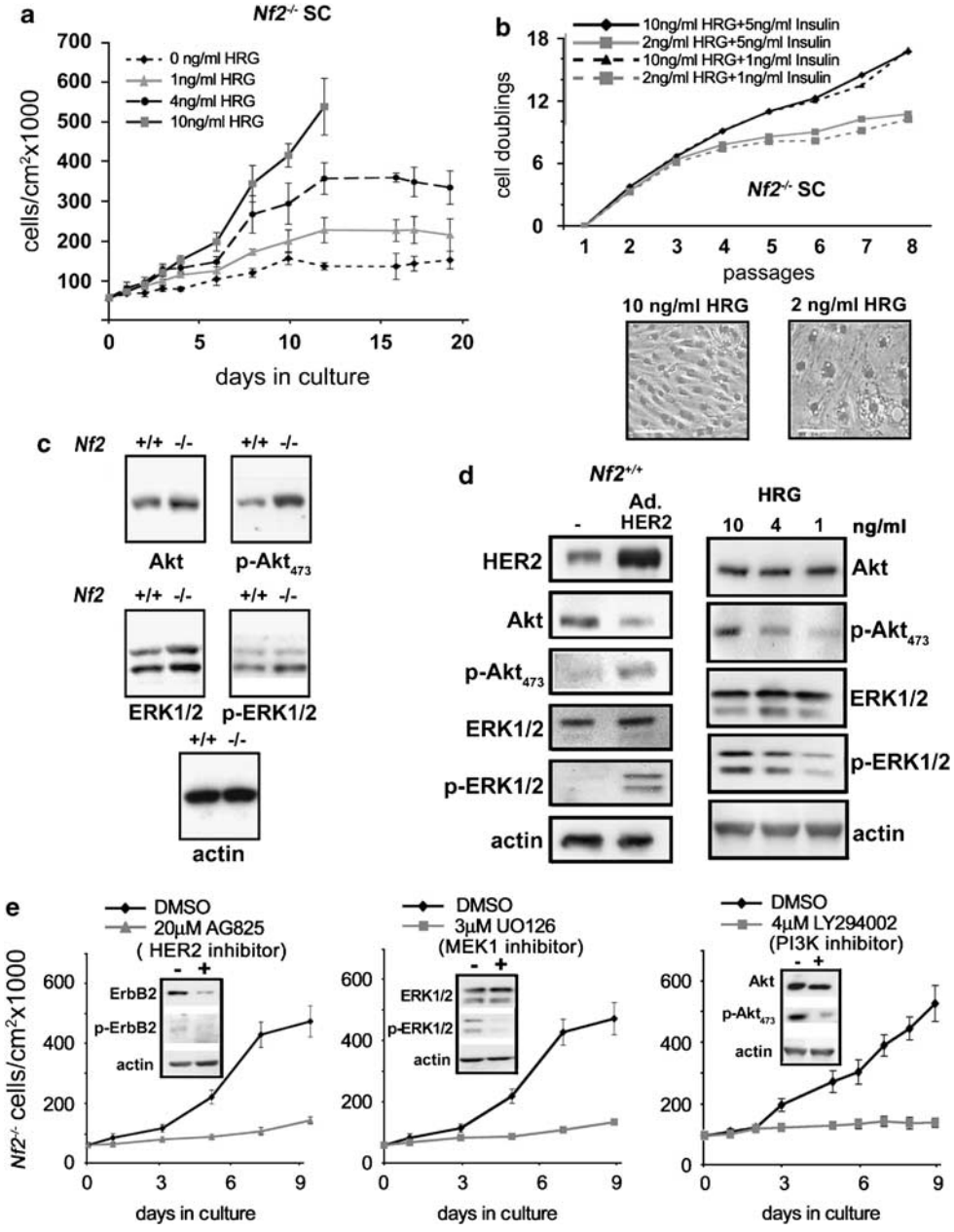

Figure 4 Analysis of the signaling pathways activated in $Nf2^{-/-}$ Schwann cells (SCs). (**a**) Growth curve of $Nf2^{-/-}$ primary SCs at passage 3 under decreasing concentrations of heregulin-β1 (HRG). (**b**) Cumulative number of $Nf2^{-/-}$ SC doublings over nine successive passages in culture media with high or low levels of heregulin and insulin. The two-phase contrast pictures show the morphology of SCs in the presence of high (10 ng/ml) or low (2 ng/ml) heregulin-β1 concentration after nine passages. Scale bars = 15 μm. (**c**) Western blot analysis of mitogen-activated protein kinase (MAPK) and acutely transforming retrovirus AKT8 in rodent T-cell lymphoma (Akt) protein levels and phosphorylation in total cell extracts from $Nf2^{+/+}$ and $Nf2^{-/-}$ primary SCs at passage 3. (**d**) (Left): activation of Akt and MAPK upon adenoviral mediated overexpression of wild-type human ErbB2 (HER2) (Ad HER2) in $Nf2^{+/+}$ SCs. (Right): western blot showing the effect of heregulin-β1 (HRG) starvation on Akt and MAPK activity in $Nf2^{-/-}$ SCs. (**e**) Inhibition of $Nf2^{-/-}$ primary SC proliferation by specific inhibitors of PI3 K (4 μM LY294002), HER2 (20 μM AG825) and MEK1 (3 μM UO126). DMSO was used as control.

proliferation (Hardy *et al*., 1992; Syroid *et al*., 1999; Cheng *et al*., 2000; Lobsiger *et al*., 2000). We showed that these receptors are also upregulated in $Nf2^{-/-}$ SCs, in mouse *Nf2*-mutant nerves and in human schwannomas. Therefore, the precise role of IGF1R and PDGFR-β in schwannoma development needs further clarification. Our results demonstrate a close link between the control of protein transport and tumorigenesis. Remarkably, other protein transport modulators, such as caveolin-1, tuberin or HIP1, have been associated with tumorigenic processes, such has tuberosclerosis and colon or prostate cancer (Rao *et al*., 2002; Hyun and Ross, 2004; Jones

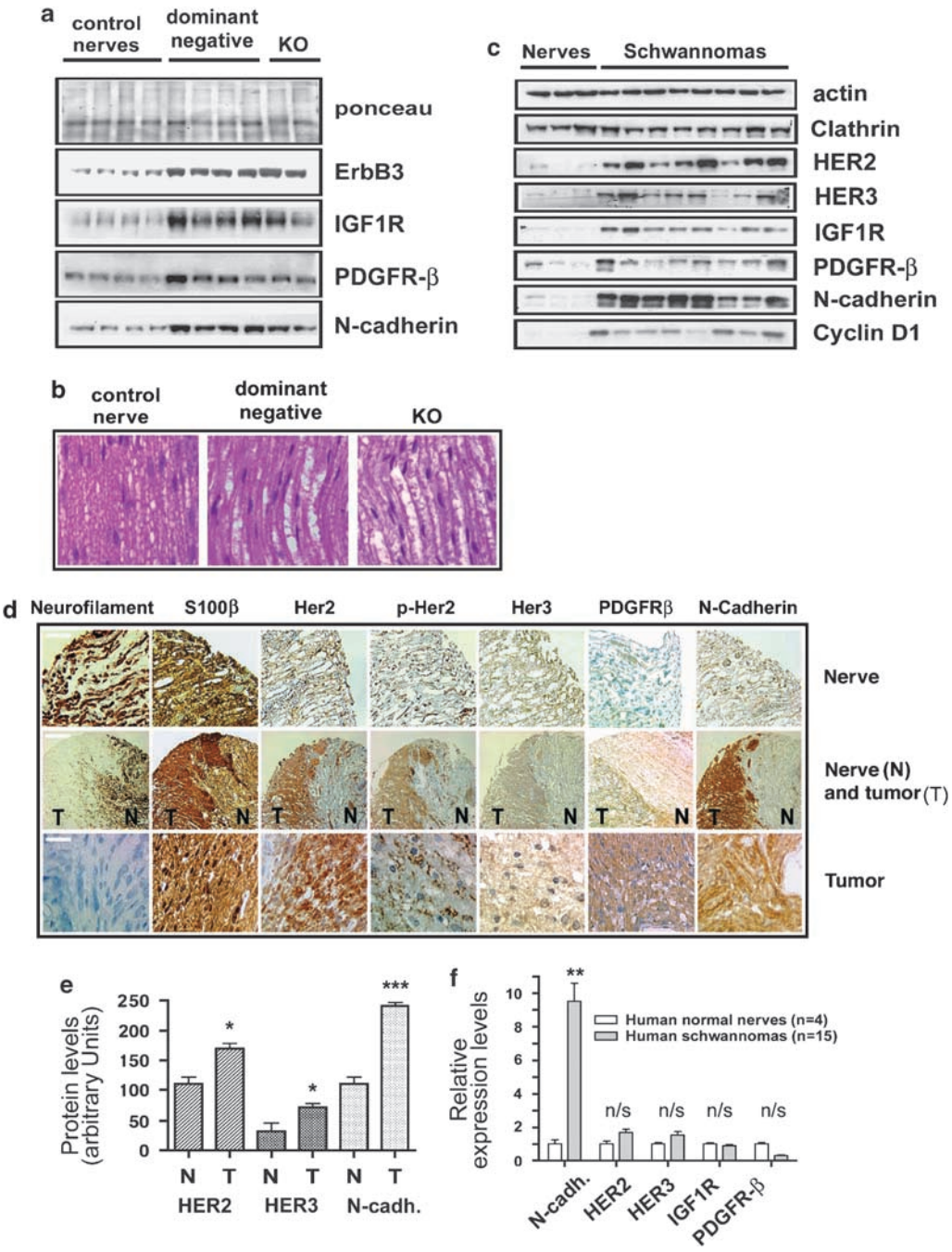

Figure 5 *Nf2*-mutant mouse nerves and human schwannomas show accumulation of plasma membrane-associated proteins. (**a**) Western blot analysis of the expression level of ErbB3, insulin-like growth factor 1 receptor (IGF1R), platelet-derived growth factor receptor (PDGFR)-β and N-cadherin in sciatic nerves from four wild-type mice (control nerves), four mice expressing a dominant negative form of *Nf2* (dominant negative) and two mice with SC-specific inactivation of *Nf2* (KO). Equal loadings were confirmed by Ponceau red staining. (**b**) Histology of the sciatic nerves analysed in (**a**) showing no apparent lesions. (**c**) Western blot analysis of expression levels of human ErbB2 (HER2) and 3 (Her3), IGF1R, PDGFR-β, N-cadherin, Cyclin D1 and clathrin in three normal human nerves (Nerves) and eight human schwannomas (three from NF2 patients (lanes 6, 10 and 11) and five from *NF2*-deficient sporadic schwannomas (lanes 4, 5, 7, 8 and 9)). Actin was used as a loading control. (**d**) Immunohistochemical staining of neurofilament, protein S100, HER2, phospho-HER2, HER3, PDGFR-β and N-cadherin in human normal nerves and schwannomas. The top panels (Nerve) show the staining of nonpathological human nerves. Scale bar = 50 μm. The middle series of panels (Nerve and tumor) show the staining of a schwannoma (T) developing from the nerve (N). Scale bar = 100 μm. The lower panels show staining of human schwannomas at higher magnification. Scale bar = 10 μm. (**e**) Quantitative analysis of the immunohistochemical staining of HER2, HER3 and N-cadherin in a series of 8 normal human nerves compared with 30 human schwannomas. The differences observed are statistically significant. (**f**) Comparison of *N-cadherin, HER2, HER3, IGF1R and PDGFR-β* mRNA expression levels in normal human nerves and human schwannomas, measured by quantitative reverse transcription–PCR. NS indicates that the differences are statistically nonsignificant ($P > 0.05$).

et al., 2004; Jozwiak, 2006). Hence, the role of these proteins in vesicular trafficking could be key to their tumor suppressing activity. As the study of dysregulated protein transport is becoming a major theme in cancer research (Bache *et al*., 2004; Polo *et al*., 2004), elucidating how the tumor suppressor merlin controls protein transport constitutes an essential contribution in this emerging field.

Materials and methods

Mouse models
The two mouse models used in our study were described previously. Briefly, in the first model, the *floxed Nf2* gene was conditionally inactivated in SCs *in vivo* by tissue-specific expression of the Cre recombinase under the control of the P0 promoter (Giovannini *et al*., 2000). In the second model, SC-specific P0 promoter was used to drive the expression of a dominant negative mutant merlin (Sch-Δ39–121) (Giovannini *et al*., 1999). This model was used for experiments involving extracts from sciatic nerves.

Cell cultures
All primary SC cultures were derived from the $Nf2^{flox/flox}$ mouse model. Primary mouse SC cultures were produced from adult $Nf2^{flox/flox}$ mouse sciatic nerves and P75-mediated cell sorting of SCs (Manent *et al*., 2003) was used for SC purification. SCs were routinely cultured in N2 media (DMEM-F12 with 2 μM forskolin, 10 ng/ml heregulin, 50 μg/ml gentamicin, 2.5 μg/ml fungizone and N2 supplement (Gibco, Invitrogen, Cergy Pontoise, France)). Cre-adenovirus-mediated *Nf2* (Ad5CMV-Cre, University of Iowa Gene Transfer Vector Core, Iowa City, IA, USA) was assessed by western blot. For each experiment, control SCs were infected with either an empty adenovirus or an adenovirus expressing β-galactosidase. For growth curves, SCs were seeded at 7.5×10^4 cells/cm^2, and counted daily. For senescence studies, SCs were seeded at 5×10^4 cells/cm^2 at each passage and counted after 7 days. The number of cell doublings (N) was calculated as follows: $N = \text{Log}\,(N_f/N_i)/\text{Log}2$. N_i is the number of plated SCs and N_f is the number of SCs counted after 1 week. Experiments were repeated at least three times.

Adenovirus production and SC infection
Merlin isoform 1 and ts045VSV-GFP adenoviruses were prepared using the Adeasy system (Stratagene, Agilent, Massy, France). Infection efficiencies close to 100% were assessed by immunofluorescence.

Protein analysis and antibodies
Total cell and membrane extract preparation were described previously (Lallemand *et al*., 2003). For mouse peripheral nerve extracts, sciatic nerves from 2- to 6.5-month-old mice were dissected and solubilized in 9 M urea by trituration on ice with an Ultrathurrax (IKA Labortechnik, Staufen, Germany) and sonicated. Debris were removed by centrifugation at 20 000 *g* (10 min at 4 °C). All mice used for analysis were FVB/N mixed strain with littermates serving as controls. Animal care and experimentation reported herein were conducted in compliance with the guidelines and with the approval of Institutional Animal Care and Use Committee of the French Department of Agriculture. The study involving human tumor samples was conducted after approval from the Comité Consultatif des Personnes Participant à une Recherche Biomedicale. Tumor and nerve samples were obtained from patients who provided informed consent. Extracts from human nerves and schwannomas were prepared in 9 M urea, as above. Protein concentration was measured by Bradford assay (Bio-Rad, Marnes la Coquette, France). For western blotting, proteins were separated by SDS–polyacrylamide gel electrophoresis (SDS–PAGE) and transferred to nitrocellulose. Membranes were incubated with primary antibodies overnight at 4 °C in phosphate-buffered saline (PBS) + 0.1% Tween and 5% nonfat dry milk, or PBS + 0.1% Tween 20 and 2% bovine serum albumin for phospho-specific antibodies. Antibodies: Cell Signaling Technology (Ozyme, Saint Quentin en Yvelines, France) (IGF1R [3027]; phospho-IGF1R [3024]; ErbB2 [2248]; phospho-ErbB2 [2241]; phospho-ErbB3 [4791]; MAPK [9102]; phospho-MAPK [9101]; Akt [9272]; phospho-Akt [9271]; PDGFR-β [3162]; $P27^{Kip}$ [2552]; Trp53 [2524]), Santa Cruz (Tebubio, Le Perray en Yvelines, France) (merlin [A-19]; ErbB3 [C-17]; N-cadherin [H63]; E-cadherin [H108]; P107 [C-18]; P130 [C-20]; $P21^{Cip}$ [F-5]; $P19^{Arf}$ [M167]; cyclin D1 [DCS-6]; Rab11[H-87]; β-actin [C-2]; GFP [B-2]), Transduction Lab (BD Bioscience, Rungis, France) (β-catenin [610154]; Lamp-1 [553792]; EE1A [61045]; P115 [612260]; clathrin [clone 23]). Horseradish peroxidase-linked secondary antibodies were from Amersham Bioscience (Saclay, France).

Immunofluorescence
Schwann cells were fixed on glass coverslips for 20 min in 4% formaldehyde, permeabilized for 10 min in PBS with 0.2% Triton X-100 and incubated overnight at 4 °C with the primary antibody in PBS plus 0.1%Tween and 10% fetal calf serum. Samples were incubated for 2 h at room temperature with the secondary antibody (Amersham Bioscience), and mounted on a glass slide using Citifluor mounting media (Citifluor Ltd, Biovalley, Marne la Vallée, France).

Schwann cell membrane quantification
A total of 5×10^6 $Nf2^{-/-}$ and $Nf2^{+/+}$ SCs were trypsinized and rinsed in PBS. After centrifugation at 500 *g* for 5 min, cells were resuspended in 3 ml of ice-cold HBSS containing 5 μg/ml of FM1-43 FX lipophylic styryl dye (Molecular Probes, Invitrogen, Cergy Pontoise, France) for 10 min on ice. Formaldehyde (4%) was added for 20 min on ice. Following two rinses in HBSS, fluorescence of the incorporated dye was quantified by fluorescence-activated cell sorting.

Cell surface proteins biotinylation
For all the experiments involving cell surface protein biotinylation, SCs were plated at 5×10^4 cells/cm^2 and grown for 5–7 days until they reached early confluence. Biotinylation of surface proteins was performed for 30 min at 4 °C using the Pinpoint Cell Surface Protein Isolation Kit (Pierce) and following instructions from the manufacturer. For experiments involving merlin re-expression, $Nf2^{-/-}$ SCs were infected with merlin (isoform I) expressing adenovirus 1 day after plating and processed as above.

Surface receptors clearance experiment
Following surface protein biotinylation pulse, confluent SCs were placed back in culture media at 37 °C for the indicated time points. Then, SCs were collected and biotinylated proteins were extracted from equal amounts of extracts following the instructions from the manufacturer.

Receptor internalization experiment
$Nf2^{-/-}$ cells were seeded at 5×10^4 cells/cm^2. After 1 day, one-half of the plates were infected with merlin-expressing

adenovirus to generate $Nf2^{-/-;adNF2}$ SCs. After 5–7 days, when cultures reached early confluence, $Nf2^{-/-}$ and $Nf2^{-/-;adNF2}$ SCs were biotinylated for 30 min at 4 °C and placed back in culture media at 37 °C for the indicated time. Then, biotin groups still exposed at the cell surface were stripped (two incubations at 4 °C in 75 mM NaCl, 50 mM NaOH, 50 mM glutathione). Internalized proteins protected from stripping and still biotinylated were purified from equal amounts of cell extracts and analysed by western blot.

ts045VSV-GFP cytoplasmic membrane delivery quantification
$Nf2^{-/-}$ SCs were infected with adenovirus expressing the ts045VSV-GFP. After 1 day, half of the culture was infected with adenovirus expressing merlin isoform 1 and the other half with a control adenovirus. After 2 days, cells were switched to 40 °C for 36 h. Then, surface proteins were biotinylated 0, 1, 2, 4 and 8 h following switch to 32 °C. Biotinylated proteins were purified from equal amounts of cell extracts for each time point, and ts045VSV-GFP expression at the surface of the cell was quantified by western blot (anti-GFP, Santa Cruz).

Immunohistochemistry
Sections of paraffin-embedded tissue (3 μm) were stained (streptavidin-peroxidase protocol, immunostainer BenchMark Ventana, Illkirch, France) with antibodies to: ErbB2 (Ab-17, LabVision, Interchim, Montluçon, France), phospho-ErbB2 (Ab-18, LabVision), S100 (PN IM1926, Immunotech, Marseille, France), neurofilament (clone 2F11, Dako, Trappes, France), PDGFR-β (Cell Signaling Technology [3162]), ErbB3 (SGP1, LabVision) and N-cadherin (H63, Santa Cruz). For quantification, 2–4 sections of each tumor or nerve were evaluated independently by two investigators (AC and DL) and the percentage of labeled cells was estimated (P). A score (I) was attributed in function of the staining intensity (0 = no staining, 1 = weak staining, 2 = moderate staining and 3 = strong staining). A final score $S = P \times I$ was calculated for each section. Statistical analysis (mean, standard error of the mean (s.e.m.) and nonparametric paired t-test) was performed using Prism software.

RNA extraction and quality control
Total RNA was extracted from confluent primary SC cultures at passage 3 using the RNeasy protocol (Qiagen, Courtaboeuf, France) with on-column Dnase I digestion (Qiagen). For schwannoma analysis, 100–200 mg of tissue was used for RNA extraction.

Total RNA from human nerves and tumors was extracted using a modified RNeasy protocol consisting of lysis in TRIzol (Invitrogen, Cergy Pontoise, France) followed by RNeasy Cleanup protocol (Qiagen). Quality of RNAs was assessed by Bioanalyser 2100 (Agilent, Massy, France). All RNAs used for further experimentation displayed a 28s/18s ratio between 1.6 and 2.1.

Quantitative RT–PCR
A total of 3 μg of total RNA was reverse-transcribed in a final volume of 100 μl using the High Capacity cDNA Archive Kit with random hexamers (Applied Biosystems, Courtaboeuf, France). TaqMan gene expression assays containing gene-specific primers and probe sets (Applied Biosystems) were used for the detection of mouse and human genes. RT–PCR and the quantification of RT–PCR products were performed and analysed with ABI Prism 7900HT Sequence Detection System (Applied Biosystems). The quality of cDNAs was assessed using a ribosomal *R18S* quantification by RT–PCR. The relative amount of measured mRNA in samples was determined using the $2^{-\Delta\Delta CT}$ method (CT = cycle threshold) where $\Delta\Delta CT = (CT_{target} - CT_{R18s})_{sample} - (CT_{target} - CT_{R18s})_{calibrator}$. Final results are expressed as the ratio $2^{-\Delta\Delta CT}$ ($Nf2^{-/-}$)/$2^{-\Delta\Delta CT}$ ($Nf2^{+/+}$), where $Nf2^{-/-}$ samples are $Nf2^{-/-}$ mouse SCs or human schwannomas and $Nf2^{+/+}$ samples are wild-type mouse SCs or human normal nerve, respectively.

Statistical analysis
Statistical analysis was performed using Prism 4 software. Results are reported as mean ± standard deviation (s.d.). Data were analysed by unpaired t-test and differences were considered significant when $P<0.05$ (***$P<0.001$, **$0.001<P<0.01$, *$0.01<P<0.05$).

Conflict of interest
None declared.

Acknowledgements

We thank J Lippincott-Schwartz for the kind gift of the VSV-GFP construct, Z-Y Han for assistance with mouse genotyping, all members of the U674 lab for helpful discussions and support, L Goutebroze B Goud and O Hanemann for helpful suggestions, A McClatchey for many stimulating discussions, M Pla (Departement d'Experimentation Animale—Institut Universitaire d'Hematologie) and the Centre de Distribution, Typage et Archivage animal for mouse housing. DL personally thanks F Mechta-Grigoriou for helpful advice and discussions and continuous support and Odette Mariani for careful reading of the manuscript. This work was supported by Grants from the US Department of Defense (W81XWH-05-1-0265), Association Neurofibromatoses et Recklinghausen, Canceropôle Ile-de France, Institut National du Cancer, ANR and INSERM.

References

Bache KG, Slagsvold T, Stenmark H. (2004). Defective downregulation of receptor tyrosine kinases in cancer. *EMBO J* **23**: 2707–2712.

Bretscher A, Edwards K, Fehon RG. (2002). ERM proteins and merlin: integrators at the cell cortex. *Nat Rev Mol Cell Biol* **3**: 586–599.

Bringold F, Serrano M. (2000). Tumor suppressors and oncogenes in cellular senescence. *Exp Gerontol* **35**: 317–329.

Buzard GS, Enomoto T, Anderson LM, Perantoni AO, Devor DE, Rice JM. (1999). Activation of neu by missense point mutation in the transmembrane domain in schwannomas induced in C3H/HeNCr mice by transplacental exposure to *N*-nitrosoethylurea. *J Cancer Res Clin Oncol* **125**: 653–659.

Cheng HL, Steinway M, Delaney CL, Franke TF, Feldman EL. (2000). IGF-I promotes Schwann cell motility and survival via activation of Akt. *Mol Cell Endocrinol* **170**: 211–215.

Curto M, Cole BK, Lallemand D, Liu CH, McClatchey AI. (2007). Contact-dependent inhibition of EGFR signaling by Nf2/Merlin. *J Cell Biol* **177**: 893–903.

Deretic D, Traverso V, Parkins N, Jackson F, Rodriguez de Turco EB, Ransom N. (2004). Phosphoinositides, ezrin/moesin, and rac1

regulate fusion of rhodopsin transport carriers in retinal photoreceptors. *Mol Biol Cell* **15**: 359–370.

Fernandez-Valle C, Tang Y, Ricard J, Rodenas-Ruano A, Taylor A, Hackler E *et al*. (2002). Paxillin binds schwannomin and regulates its density-dependent localization and effect on cell morphology. *Nat Genet* **31**: 354–362.

Fraenzer JT, Pan H, Minimo Jr L, Smith GM, Knauer D, Hung G. (2003). Overexpression of the NF2 gene inhibits schwannoma cell proliferation through promoting PDGFR degradation. *Int J Oncol* **23**: 1493–1500.

Giovannini M, Robanus-Maandag E, Niwa-Kawakita M, van der Valk M, Woodruff JM, Goutebroze L *et al*. (1999). Schwann cell hyperplasia and tumors in transgenic mice expressing a naturally occurring mutant NF2 protein. *Genes Dev* **13**: 978–986.

Giovannini M, Robanus-Maandag E, van der Valk M, Niwa-Kawakita M, Abramowski V, Goutebroze L *et al*. (2000). Conditional biallelic Nf2 mutation in the mouse promotes manifestations of human neurofibromatosis type 2. *Genes Dev* **14**: 1617–1630.

Hansen MR, Linthicum Jr FH. (2004). Expression of neuregulin and activation of erbB receptors in vestibular schwannomas: possible autocrine loop stimulation. *Otol Neurotol* **25**: 155–159.

Hardy M, Reddy UR, Pleasure D. (1992). Platelet-derived growth factor and regulation of Schwann cell proliferation *in vivo*. *J Neurosci Res* **31**: 254–262.

Hirokawa Y, Tikoo A, Huynh J, Utermark T, Hanemann CO, Giovannini M *et al* (2004). A clue to the therapy of neurofibromatosis type 2: NF2/merlin is a PAK1 inhibitor. *Cancer J* **10**: 20–26.

Hirschberg K, Miller CM, Ellenberg J, Presley JF, Siggia ED, Phair RD *et al* (1998). Kinetic analysis of secretory protein traffic and characterization of golgi to plasma membrane transport intermediates in living cells. *J Cell Biol* **143**: 1485–1503.

Hyun TS, Ross TS. (2004). HIP1: trafficking roles and regulation of tumorigenesis. *Trends Mol Med* **10**: 194–199.

Itahana K, Campisi J, Dimri GP. (2004). Mechanisms of cellular senescence in human and mouse cells. *Biogerontology* **5**: 1–10.

Jones KA, Jiang X, Yamamoto Y, Yeung RS. (2004). Tuberin is a component of lipid rafts and mediates caveolin-1 localization: role of TSC2 in post-Golgi transport. *Exp Cell Res* **295**: 512–524.

Jozwiak J. (2006). Hamartin and tuberin: working together for tumour suppression. *Int J Cancer* **118**: 1–5.

Kissil JL, Wilker EW, Johnson KC, Eckman MS, Yaffe MB, Jacks T. (2003). Merlin, the product of the Nf2 tumor suppressor gene, is an inhibitor of the p21-activated kinase, Pak1. *Mol Cell* **12**: 841–849.

Lallemand D, Curto M, Saotome I, Giovannini M, McClatchey AI. (2003). NF2 deficiency promotes tumorigenesis and metastasis by destabilizing adherens junctions. *Genes Dev* **17**: 1090–1100.

Lim JY, Kim H, Kim YH, Kim SW, Huh PW, Lee KH *et al*. (2003). Merlin suppresses the SRE-dependent transcription by inhibiting the activation of Ras-ERK pathway. *Biochem Biophys Res Commun* **302**: 238–245.

Lobsiger CS, Schweitzer B, Taylor V, Suter U. (2000). Platelet-derived growth factor-BB supports the survival of cultured rat Schwann cell precursors in synergy with neurotrophin-3. *Glia* **30**: 290–300.

Maitra S, Kulikauskas RM, Gavilan H, Fehon RG. (2006). The tumor suppressors Merlin and Expanded function cooperatively to modulate receptor endocytosis and signaling. *Curr Biol* **16**: 702–709.

Manent J, Oguievetskaia K, Bayer J, Ratner N, Giovannini M. (2003). Magnetic cell sorting for enriching Schwann cells from adult mouse peripheral nerves. *J Neurosci Methods* **123**: 167–173.

Mary S, Charrasse S, Meriane M, Comunale F, Travo P, Blangy A *et al*. (2002). Biogenesis of N-cadherin-dependent cell–cell contacts in living fibroblasts is a microtubule-dependent kinesin-driven mechanism. *Mol Biol Cell* **13**: 285–301.

McClatchey AI, Giovannini M. (2005). Membrane organization and tumorigenesis—the NF2 tumor suppressor, Merlin. *Genes Dev* **19**: 2265–2277.

Miyake K, McNeil PL, Suzuki K, Tsunoda R, Sugai N. (2001). An actin barrier to resealing. *J Cell Sci* **114**: 3487–3494.

Morrison H, Sperka T, Manent J, Giovannini M, Ponta H, Herrlich P. (2007). Merlin/neurofibromatosis type 2 suppresses growth by inhibiting the activation of Ras and Rac. *Cancer Res* **67**: 520–527.

Muallem S, Kwiatkowska K, Xu X, Yin HL. (1995). Actin filament disassembly is a sufficient final trigger for exocytosis in nonexcitable cells. *J Cell Biol* **128**: 589–598.

Nikitin A, Ballering LA, Lyons J, Rajewsky MF. (1991). Early mutation of the neu (erbB-2) gene during ethylnitrosourea-induced oncogenesis in the rat Schwann cell lineage. *Proc Natl Acad Sci USA* **88**: 9939–9943.

Perrais M, Chen X, Perez-Moreno M, Gumbiner BM. (2007). E-cadherin homophilic ligation inhibits cell growth and epidermal growth factor receptor signaling independently of other cell interactions. *Mol Biol Cell* **18**: 2013–2025.

Polo S, Pece S, Di Fiore PP. (2004). Endocytosis and cancer. *Curr Opin Cell Biol* **16**: 156–161.

Pujuguet P, Del Maestro L, Gautreau A, Louvard D, Arpin M. (2003). Ezrin regulates E-cadherin-dependent adherens junction assembly through Rac1 activation. *Mol Biol Cell* **14**: 2181–2191.

Qian X, Karpova T, Sheppard AM, McNally J, Lowy DR. (2004). E-cadherin-mediated adhesion inhibits ligand-dependent activation of diverse receptor tyrosine kinases. *EMBO J* **23**: 1739–1748.

Rao DS, Hyun TS, Kumar PD, Mizukami IF, Rubin MA, Lucas PC *et al*. (2002). Huntingtin-interacting protein 1 is overexpressed in prostate and colon cancer and is critical for cellular survival. *J Clin Invest* **110**: 351–360.

Sherman L, Sleeman JP, Hennigan RF, Herrlich P, Ratner N. (1999). Overexpression of activated neu/erbB2 initiates immortalization and malignant transformation of immature Schwann cells *in vitro*. *Oncogene* **18**: 6692–6699.

Siskova Z, Baron W, de Vries H, Hoekstra D. (2006). Fibronectin impedes 'myelin' sheet-directed flow in oligodendrocytes: a role for a beta 1 integrin-mediated PKC signaling pathway in vesicular trafficking. *Mol Cell Neurosci* **33**: 150–159.

Stanasila L, Abuin L, Diviani D, Cotecchia S. (2006). Ezrin directly interacts with the alpha1b-adrenergic receptor and plays a role in receptor recycling. *J Biol Chem* **281**: 4354–4363.

Stonecypher MS, Chaudhury AR, Byer SJ, Carroll SL. (2006). Neuregulin growth factors and their ErbB receptors form a potential signaling network for schwannoma tumorigenesis. *J Neuropathol Exp Neurol* **65**: 162–175.

Syroid DE, Zorick TS, Arbet-Engels C, Kilpatrick TJ, Eckhart W, Lemke G. (1999). A role for insulin-like growth factor-I in the regulation of Schwann cell survival. *J Neurosci* **19**: 2059–2068.

Tamma G, Klussmann E, Oehlke J, Krause E, Rosenthal W, Svelto M *et al*. (2005). Actin remodeling requires ERM function to facilitate AQP2 apical targeting. *J Cell Sci* **118**: 3623–3630.

Supplementary Information accompanies the paper on the Oncogene website (http://www.nature.com/onc)